# Supporting information

## Three-dimensional N-doped super-hydrophilic carbon electrodes with porosity tailored by $Cu_2O$ template-assisted electrochemical oxidation to improve performance of electrical double-layer capacitors

Xiaowei Lv,[a] Shan Ji,[*b] Vladimir Linkov,[c] Xuyun Wang,[a] Hui Wang,[*a,d] and Rongfang Wang[a]

[a] State Key Laboratory Base for Eco-Chemical Engineering, College of Chemical Engineering, Qingdao University of Science and Technology, Qingdao, 266042, China.

[b] College of Biological, Chemical Science and Engineering, Jiaxing University, Jiaxing, 314001, China.

[c] South African Institute for Advanced Materials Chemistry, University of the Western Cape, Cape Town, 7535, South Africa.

[d] Guangdong Provincial Key Laboratory for Electronic Functional Materials and Devices, Huizhou University, Huizhou, 516007, P. R. China

### Physical characterizations

The images of scanning electron microscopy (SEM) were taken on JSM-6330F. The SL200B instrument was used to measure the surface wettability of different samples. The XRD patterns of the catalysts were recorded on a Shimadzu XD-3A (Japan), using filtered Cu-Kα radiation (λ =0.15418 nm), generated at 40 kV and 30

mA. X-ray photoelectron spectra (XPS) was acquired with a VG Escalab210 spectrometer fitted with Mg 300 W X-ray source. Transmission electron micrographs (TEM), high angle annular dark field scanning transmission electron microscopy (STEM) images and selected area electron diffraction (SAED) patterns of the catalysts were obtained using a JEOL (JEM-2000 FX) microscope operating at 200 kV. Energy dispersive spectroscopy (EDS) in the STEM mode was employed for determining the elemental composition of either individual particles or several particles. The specific surface area was determined by Brunauer-Emmette-Teller (BET) method and the pore size distribution was calculated by the density functional theory (DFT) method using the model slit pore, NLDFT equilibrium model on a Quantachrome Autosorb-1 volumetric analyzer. Record the conductivity on the ROOKO four-probe resistivity tester (FT-7200A).

**Electrochemical measurements**

All electrochemical tests of the as-prepared samples were evaluated on the CHI 660E electrochemical workstation. The obtained sample (size: 1×1 $cm^2$), platinum foil, Ag/AgCl (saturated KCl) were employed as the working electrode, the counter electrode, and the reference electrode respectively. $H_2SO_4$ (1 M) was used as the electrolyte for all electrochemical tests. The calculation methods of area specific capacitance ($C_a$), volume specific capacitance ($C_v$), energy density (E) and power density (P) were described in detail bellow:

Area specific capacitance ($C_a$), volume specific capacitance ($C_v$), energy density (E) and power density (P) were calculated by the following equations:

$$C_a = I \times t / (A \times \Delta V) \quad S(1)$$

$$C_v = I \times t / (V \times \Delta V) \quad S(2)$$

$$E = C_v \times (\Delta U)^2 / 2 \quad S(3)$$

$$P = E / \Delta t \quad S(4)$$

in which I, t, ΔV, V and A are discharge current (A), discharge time (s), potential window (ΔV) , electrode volume ($cm^3$) and electrode area ($cm^2$).

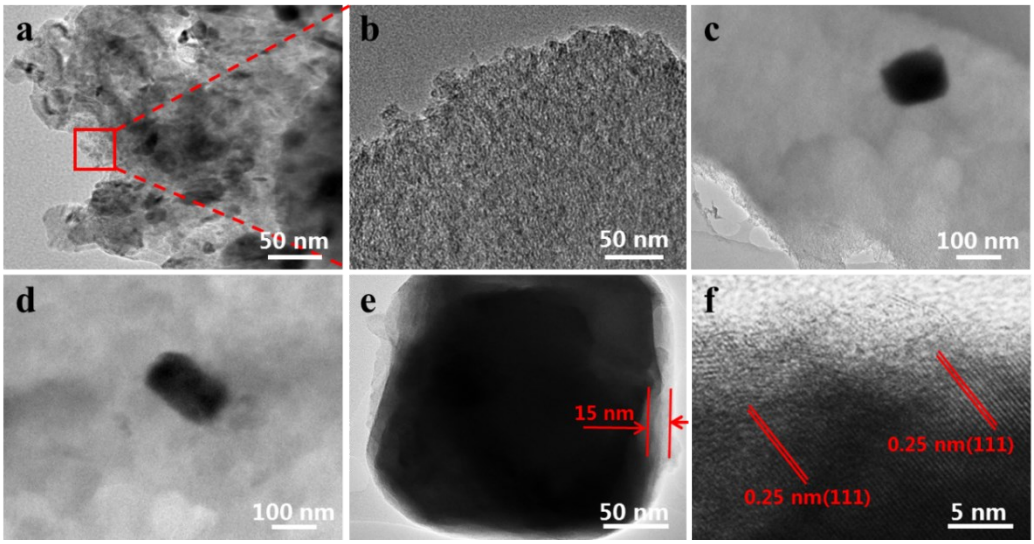


**Fig. S1** TEM images of $Cu_2O$-NCC (a); carbon layer (b); $Cu_2O$ (c-e); High-resolution TEM of $Cu_2O$ (f).

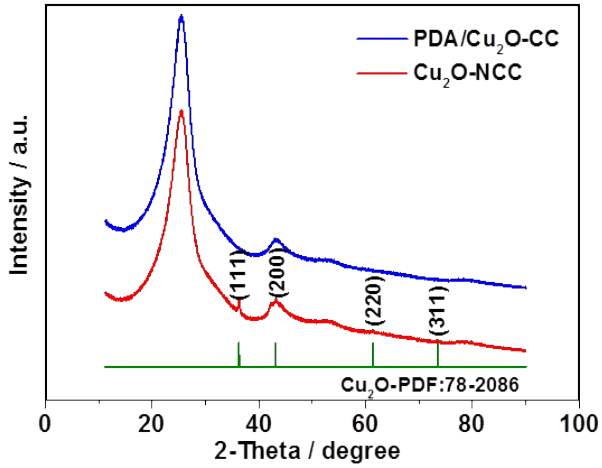

**Fig. S2** XRD patterns of PDA/$Cu_2O$-CC and $Cu_2O$-NCC.

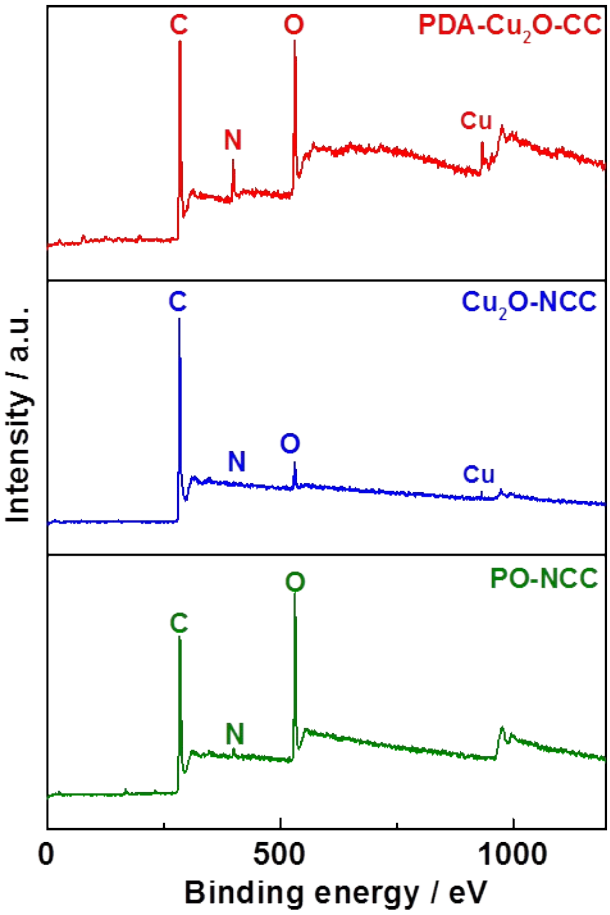


**Fig. S3** Survey XPS spectra of PDA/$Cu_2O$-CC, $Cu_2O$-NCC and PO-NCC.

As shown in Fig. S3, there are C, N, O and Cu elements existed in PDA/$Cu_2O$-CC and $Cu_2O$-NCC, and only C, N and O elements in PO-NCC, indicating that $Cu_2O$ is present on the surface of PDA/$Cu_2O$-CC and $Cu_2O$-NCC, but no Cu signal is detected on the PO-NCC, implying electrochemical oxidation at 3 V can completely remove $Cu_2O$ particles embedded in the N-doped carbon layer. The O peak of PO-NCC is very high compared to that of PDA/$Cu_2O$-CC and $Cu_2O$-NCC, implying that plenty of

oxygen functional groups formed on its surface.

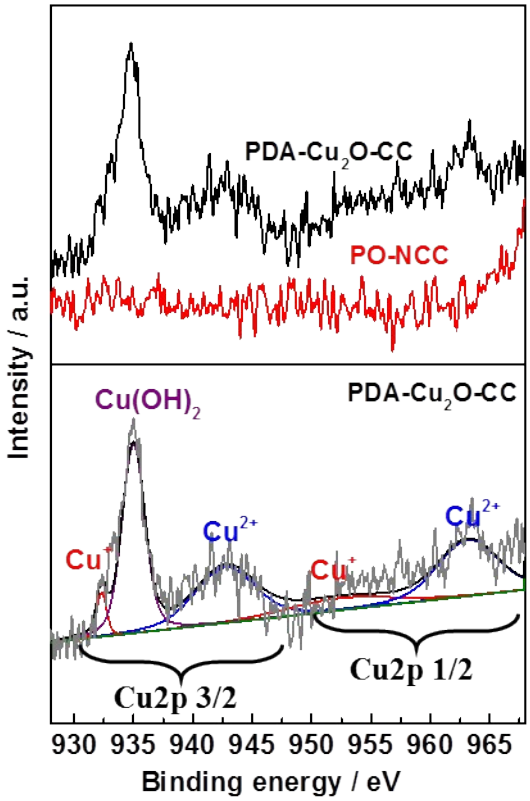


**Fig. S4** Cu 2p XPS spectra of PDA/$Cu_2O$-CC and PO-NCC.

In the Cu 2p energy spectrum of PDA/$Cu_2O$-CC, there are obvious Cu(I) characteristic peaks (Fig. S4). Cu $2p_{3/2}$ and Cu $2p_{1/2}$ peaks of PDA/$Cu_2O$-CC appear at 932.3 eV and 952.3 eV, respectively, which are consistent with the Cu(I) oxidation state of $Cu_2O$ [1]. The characteristic peaks of Cu species weren't detected in PO-NCC, confirming that $Cu_2O$ nanoparticles were completely removed during the electrochemical oxidation process.

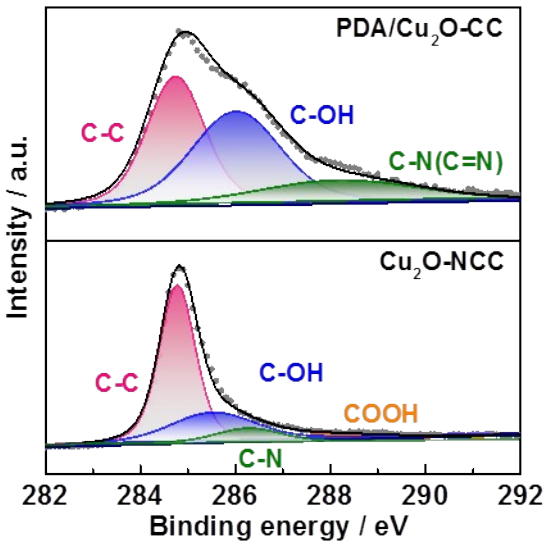


**Fig. S5** C 1s XPS spectrum of PDA/$Cu_2O$-CC and $Cu_2O$-NCC.

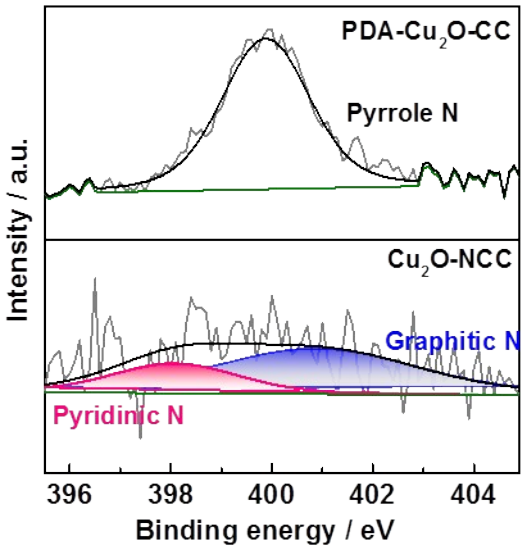


**Fig. S6** N 1s XPS spectrum of PDA/$Cu_2O$-CC and $Cu_2O$-NCC.

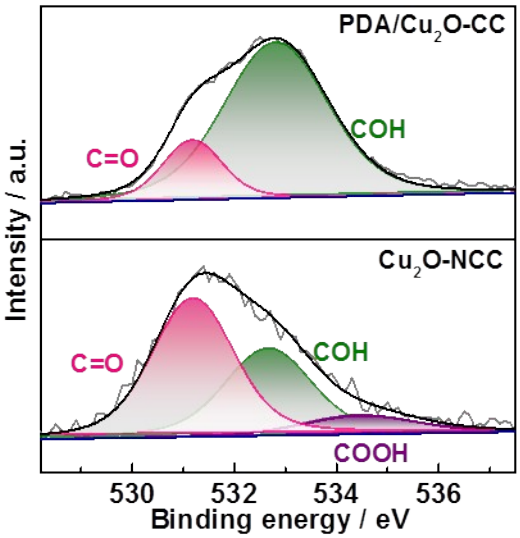


**Fig. S7** O 1s XPS spectrum of PDA/$Cu_2O$-CC, $Cu_2O$-NCC and PO-NCC.

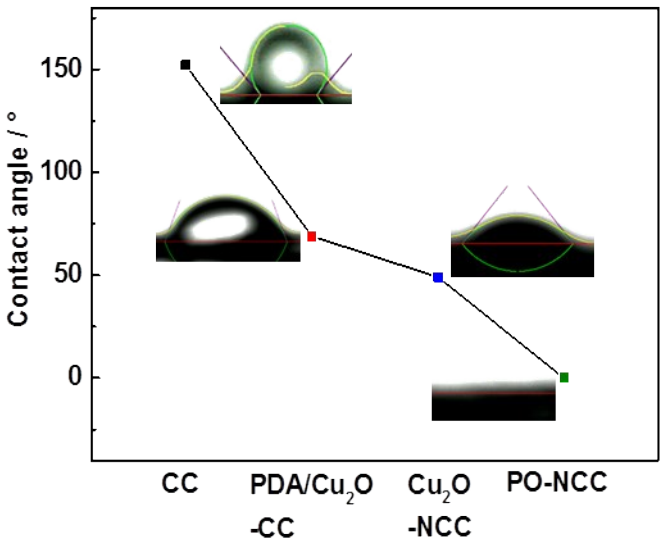


**Fig. S8** Contact angles of water micro-droplet on CC, PDA/$Cu_2O$-CC, $Cu_2O$-NCC and PO-NCC.

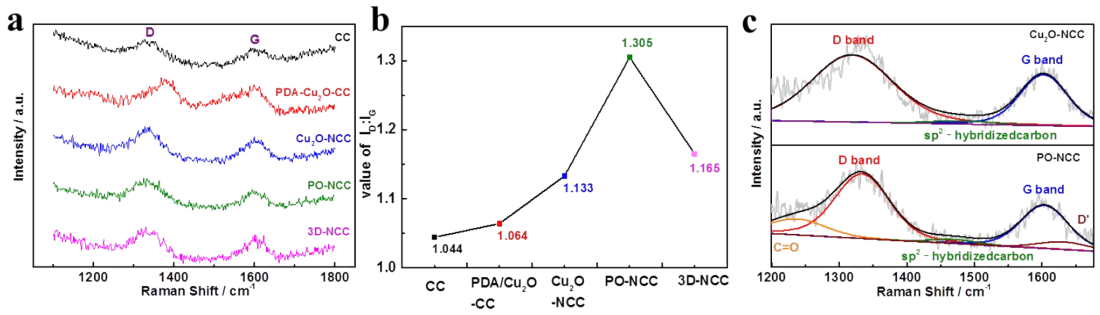


**Fig. S9** Raman spectra (a); Intensity ratios of D:G (b); fitted Raman spectra (c) of $Cu_2O$-NCC and PO-NCC.

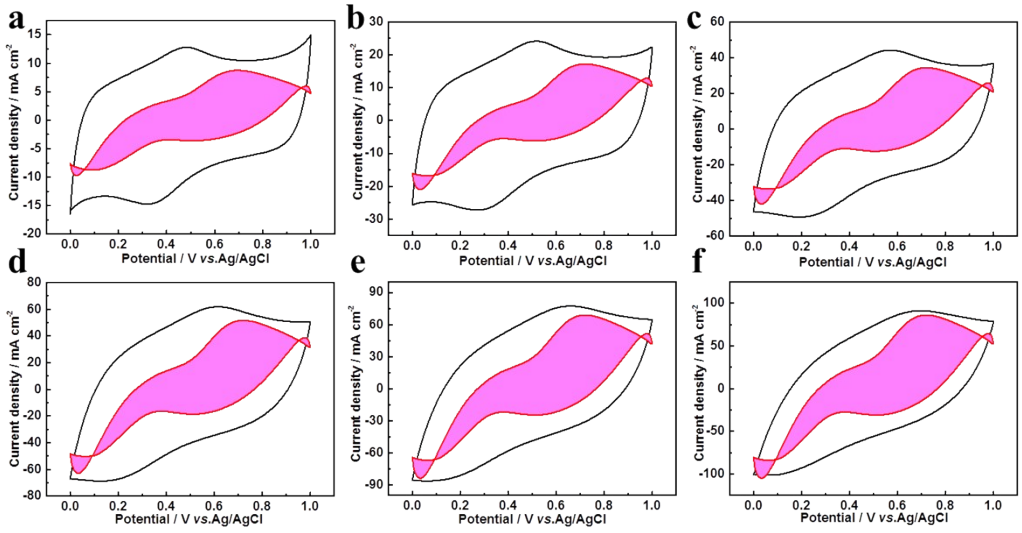


**Fig. S10** Contribution of the electric double-layer capacitance of PO-NCC at scan rates of 5,10, 20, 30, 40, and 50 mV s-1 (a-f).

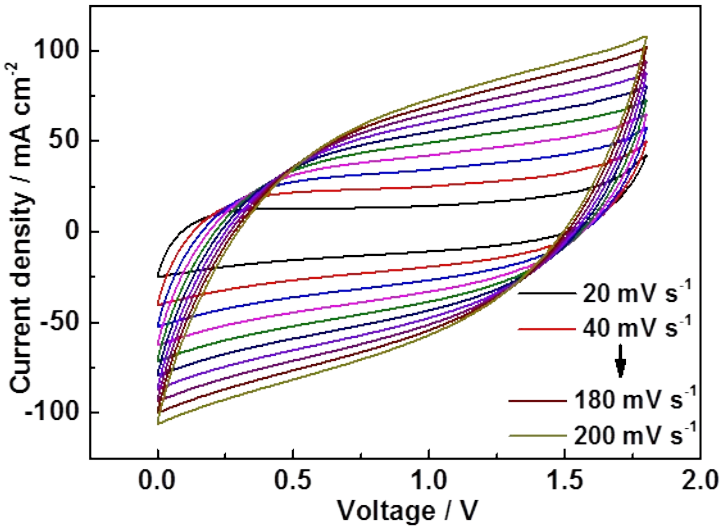


**Fig. S11** CV curves of electric double layers capacitors assembled with the PO-NCC electrodes as anode and cathode.

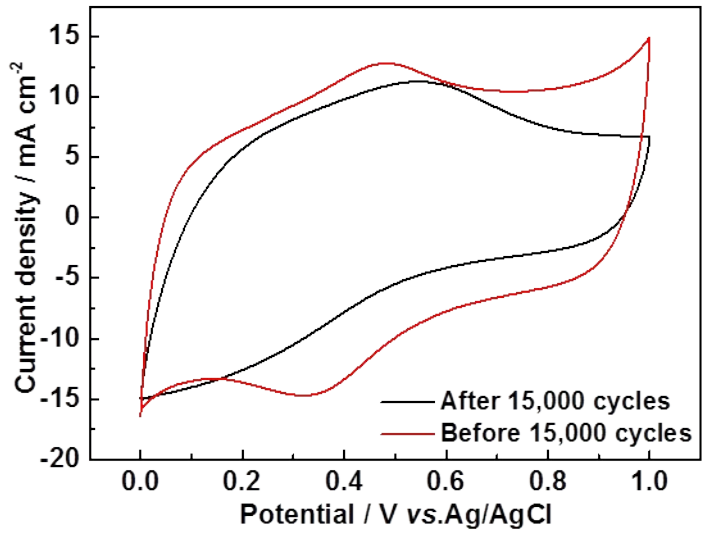


**Fig. S12** CV curve of PO-NCC after 15,000 cycles.

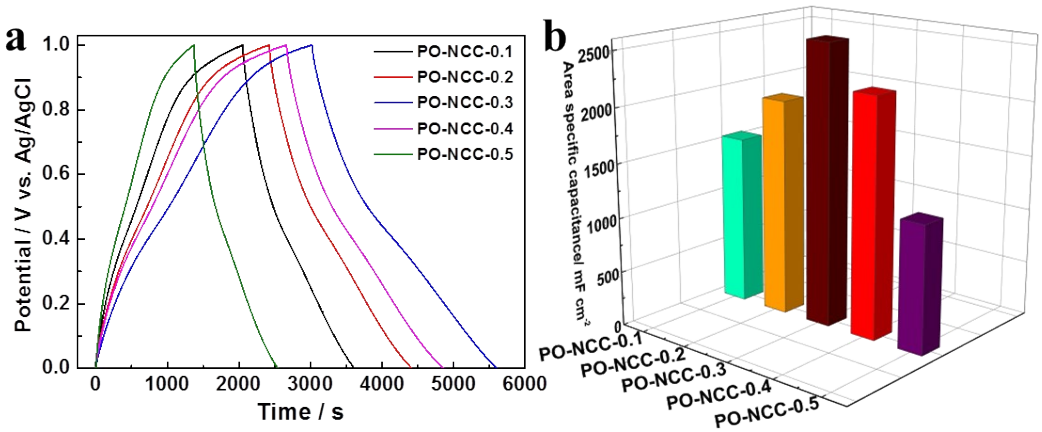


**Fig. S13** PO-NCC-m(m=0.1-0.5 mmol) charge and discharge curve(a) and area specific capacitance(b).

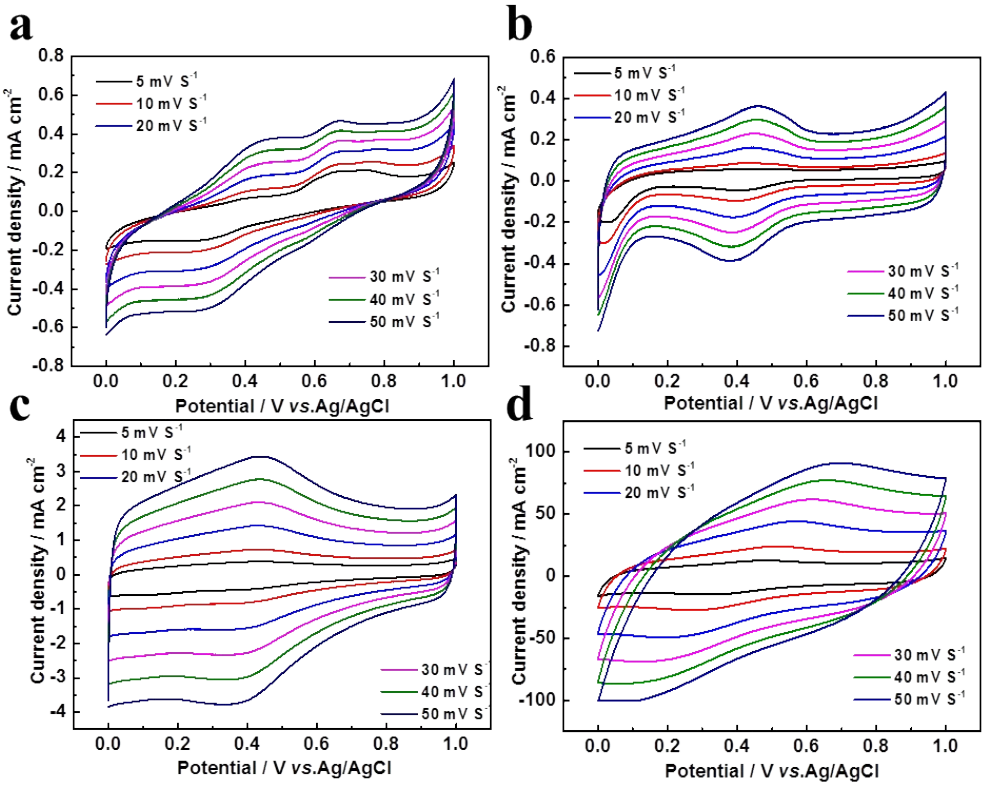


**Fig. S14** CV curves of PDA/$Cu_2O$-CC (a), $Cu_2O$-NCC (b), 3D-NCC (c) and PO-NCC (d)

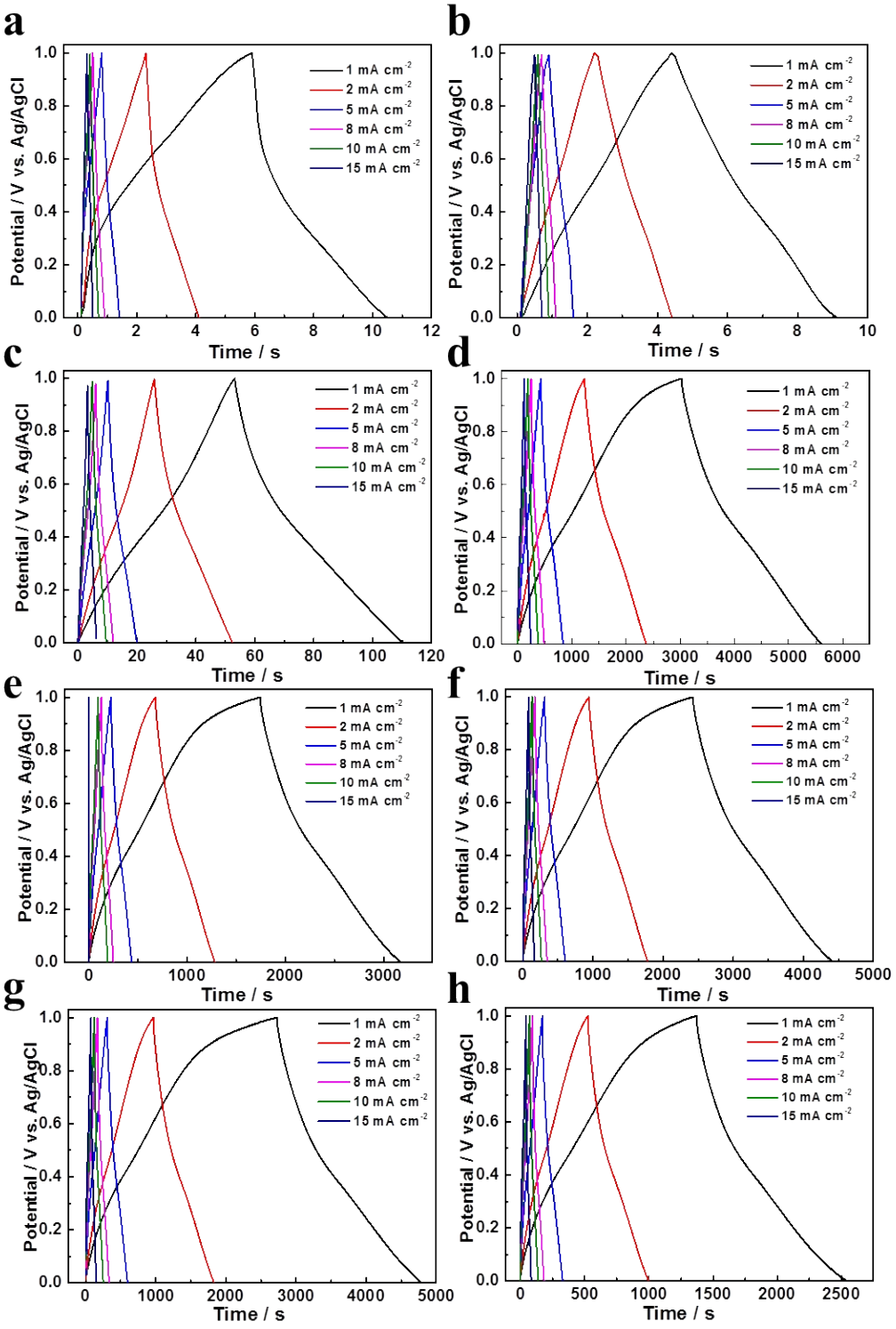


**Fig. S15** Charge and discharge curves of PDA/$Cu_2O$-CC(a), $Cu_2O$-NCC (b),3D-NCC (c), PO-NCC (d), PO-NCC-0.1(e), PO-NCC-0.2(f), PO-NCC-0.4(g) and PO-NCC-0.5(h).

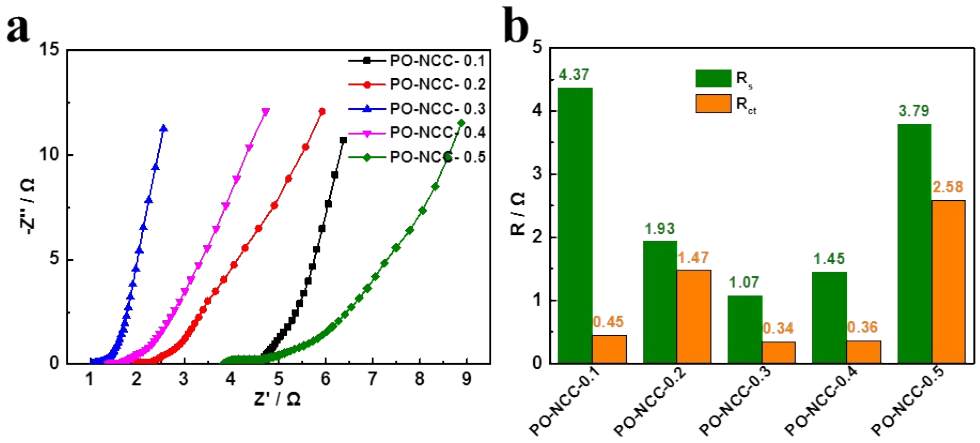


**Fig. S16** Electrochemical impedance spectra (a); calculated resistances (b).

**Table S1**. The content of oxygen functional groups on PDA/$Cu_2O$-CC，$Cu_2O$-NCC and PO-NCC based on the fitted peak areas of O 1s XPS.

| OCFG / Sample | C=O | —COH | —COOH |
|---|---|---|---|
| | Integral area (the content) | | |
| PDA/$Cu_2O$-CC | 2993.5(18%) | 13626.4(82%) | none |
| $Cu_2O$-NCC | 3221.2(54%) | 2123.8(35.6%) | 615(10.4%) |
| PO-NCC | 1537.9(7.3%) | 14027.5(66.2%) | 5631.9(26.5%) |

The percentage of each oxygen-containing functional group in brackets

**Table S2.** The conductivity of as-prepared samples.

| Sample | CC | PDA/$Cu_2O$-CC | $Cu_2O$-NCC | PO-NCC |
|---|---|---|---|---|
| Conductivity | 2.7 S/cm | 0.038 S/mm | 35.6 S/mm | 17.8 S/mm |

**Table S3.** Benchmarking the capacitor performance of as-prepared carbon electrode with the reported carbon electrodes in terms of specific capacitance, energy density, power enerngy and cycle life.

| Electroactive material | Current density | Specific Capacitance | Energy density | Power density | Electrolyte | Percentage | Cycle number | Reference |
|---|---|---|---|---|---|---|---|---|
| PO-NCC | 1 mA $cm^{-2}$ | 2582 mF $cm^{-2}$ | 16.4 mWh $cm^{-3}$ | 180 mW $cm^{-3}$ | 1 M $H_2SO_4$ | 89% | 15000 | This work |
| TCC | 2.5 mA $cm^{-2}$ | 2367 mF $cm^{-2}$ | 1.4 mWh $cm^{-3}$ | 10 mW $cm^{-3}$ | 6M KOH | 100% | 10000 | [1] |
| NCC | 12 mA $cm^{-2}$ | 1049 mF $cm^{-2}$ | 23.51 mWh $cm^{-3}$ | 1808 mW $cm^{-3}$ | 6M KOH | 92% | 10000 | [2] |
| PCC@NMC | 4 mA $cm^{-2}$ | 2680 mF $cm^{-2}$ | 4.51 mWh $cm^{-3}$ | 333.3 mW $cm^{-3}$ | 1 M $Na_2SO_4$ | no decay | 40000 | [3] |
| RPCF / CC | 12 mA $cm^{-2}$ | 1049 mF $cm^{-2}$ | 10.07 mWh $cm^{-3}$ | 55.8 mW $cm^{-3}$ | 1 M $Na_2SO_4$ | 98.4% | 6000 | [4] |
| NCNF / CC | 1 mA $cm^{-2}$ | 608 mF $cm^{-2}$ | 19.5 Wh $kg^{-1}$ | 4.1 kW $kg^{-1}$ | 2 M KOH | | 10000 | [5] |
| PNC | 2 mA $cm^{-2}$ | 682.8 mF $cm^{-2}$ | | | 1 M KOH | 96% | 10000 | [6] |
| EACC-10 | 6 mA $cm^{-2}$ | 756 mF $cm^{-2}$ | 1.5 mWh $cm^{-3}$ | 1.71 W $cm^{-3}$ | 1 M $H_2SO_4$ | 100% | 30000 | [7] |
| APCFT | 4 mA $cm^{-2}$ | 1200 mF $cm^{-2}$ | 4.7 mWh $cm^{-3}$ | 2.0 W $cm^{-3}$ | 1M $H_2SO_4$ | no any decay | 25000 | [8] |
| Activate CC | 10 mA $cm^{-2}$ | 88 mF $cm^{-2}$ | | | 1M $H_2SO_4$ | 95% | 20000 | [9] |
| AECC | 5 mA $cm^{-2}$ | 531 mF $cm^{-2}$ | 4.27 mWh $cm^{-3}$ | 1.32 W $cm^{-3}$ | 1M $H_2SO_4$ | 93% | 5000 | [10] |

## Reference


1. Wang, H.; Deng, J.; Xu, C.; Chen, Y.; Xu, F.; Wang, J.; Wang, Y., Ultramicroporous carbon cloth for flexible energy storage with high areal capacitance. Energy Storage Materials 2017, 7, 216-221.
2. Han, X.; Zhang, Y.; Wan, J.; Xu, W.; Li, J.; Hu, C.; Liu, G.; Cheng, X., An activated carbon cloth anode obtained with a fast molten salt method for high-performance supercapacitors. *Journal of Alloys and Compounds* **2020,** *838*.
3. Zhang, Q.; Sun, B.; Sun, J.; Wang, N.; Hu, W., N-doped mesoporous carbon derived from electrodeposited polypyrrole on porous carbon cloth for high-performance flexibility supercapacitors. *Journal of Electroanalytical Chemistry* **2019,** *839*, 39-47.
4. Zhang, J.; Li, W.; Ahmed Shifa, T.; Sun, J.; Jia, C.; Zhao, Y.; Cui, Y., Hierarchical porous carbon foam supported on carbon cloth as high-performance anodes for aqueous supercapacitors. *Journal of Power Sources* **2019,** *439*.
5. Liu, Y.-N.; Zhang, J.-N.; Wang, H.-T.; Kang, X.-H.; Bian, S.-W., Boosting the electrochemical performance of carbon cloth negative electrodes by constructing hierarchically porous nitrogen-doped carbon nanofiber layers for all-solid-state asymmetric supercapacitors. *Materials Chemistry Frontiers* **2019,** *3* (1), 25-31.
6. Mao, Z.; Zhao, S.; Wang, J.; Zeng, Y.; Lu, X.; Tong, Y., Facile synthesis of nitrogen-doped porous carbon as robust electrode for supercapacitors. *Materials Research Bulletin* **2018,** *101*, 140-145.
7. Wang, W.; Liu, W.; Zeng, Y.; Han, Y.; Yu, M.; Lu, X.; Tong, Y., A Novel Exfoliation Strategy to Significantly Boost the Energy Storage Capability of Commercial Carbon Cloth. *Adv Mater* **2015,** *27* (23), 3572-8.
8. Han, Y.; Lu, Y.; Shen, S.; Zhong, Y.; Liu, S.; Xia, X.; Tong, Y.; Lu, X., Enhancing the Capacitive Storage Performance of Carbon Fiber Textile by Surface and Structural Modulation for Advanced Flexible Asymmetric Supercapacitors. *Advanced Functional Materials* **2019,** *29* (7).
9. Wang, G.; Wang, H.; Lu, X.; Ling, Y.; Yu, M.; Zhai, T.; Tong, Y.; Li, Y., Solid-state supercapacitor based on activated carbon cloths exhibits excellent rate capability. *Adv Mater* **2014,** *26* (17), 2676-82, 2615.
10. Miao, Z.; Huang, Y.; Xin, J.; Su, X.; Sang, Y.; Liu, H.; Wang, J. J., High-Performance Symmetric Supercapacitor Constructed Using Carbon Cloth Boosted by Engineering Oxygen-Containing Functional Groups. *ACS Appl Mater Interfaces* **2019,** *11* (19), 18044-18050.